Normal modes in model jammed systems in three dimensions

Leonardo E. Silbert,[1] Andrea J. Liu,[2] and Sidney R. Nagel[3]
[1]*Department of Physics, Southern Illinois University, Carbondale, Illinois 62901, USA*
[2]*Department of Physics and Astronomy, University of Pennsylvania, Philadelphia, Pennsylvania 19104, USA*
[3]*James Franck Institute, University of Chicago, Chicago, Illinois 60637, USA*
(Received 15 May 2007; revised manuscript received 9 January 2009; published 27 February 2009)

Vibrational spectra and normal modes of mechanically stable particle packings in three dimensions are analyzed over a range of compressions, from near the jamming transition, where the packings lose their rigidity, to far above it. At high frequency, the normal modes are localized at all compressions. At low frequency, the nature of the modes depends somewhat on compression. At large compressions, far from the transition, the lowest-frequency normal modes have some plane-wave character, though less than one would expect for a crystalline or isotropic solid. At low compressions near the jamming transition, the lowest-frequency modes are neither plane-wave-like nor localized. We characterize these differences, highlighting the unusual dispersion behavior that emerges for marginally jammed solids.

DOI: 10.1103/PhysRevE.79.021308 PACS number(s): 81.05.Rm, 63.50.−x, 83.80.Iz, 64.70.P−

I. INTRODUCTION

It is well recognized that the high-frequency vibrations in amorphous materials are strikingly different from those in crystals. In glasses and other amorphous solids, the highest-frequency normal modes are localized in space, while in crystals they are extended excitations [1–3]. It is also appreciated that even at low frequencies the normal modes of disordered systems can be dramatically different from the long-wavelength plane waves found in ordered materials. The vibrational spectra of amorphous solids are characterized by "boson peaks"—extra low-frequency modes beyond the long-wavelength plane-wave phonons found in crystals. The anomalous modes that fall within the boson peak are believed to be responsible for the unusual low-temperature properties of glasses, such as the plateau in the thermal conductivity [4,5].

Nowhere are the excess low-frequency excitations more apparent than in a marginally jammed solid, in which a system of particles is compressed to the point where they first begin to touch and form a rigid structure [6–14]. In this system, the density of normal modes, instead of vanishing as the frequency is lowered toward zero, as in a crystal, remains constant as shown in Fig. 1(a). This excess in the density of states can be interpreted as a diverging boson peak (see Fig. 1 in Ref. [9]). Thus, one might expect the marginally jammed solid to provide the clearest window into the anomalous low-frequency normal modes characteristic of all amorphous solids.

Previously, we have found that the characteristic frequency and size of the boson peak can be tuned systematically by compressing the marginally jammed solid to higher packing fractions [9]. In the present paper we analyze the structure of the normal modes of disordered packings in three dimensions (3D) in the marginally jammed state and at compressions above this state. We examine the nature of the modes over the range of frequencies in which the density of vibrational states changes character.

II. SIMULATION MODEL

The system we study here is identical to the one used previously to calculate the density of vibrational states [8,9,15]. We simulate a 3D system of N monodisperse soft spheres of mass m and diameter σ in cubic simulation cells employing periodic boundary conditions [8]. The particles interact via a finite-range, purely repulsive, harmonic potential

$$V(r) = \begin{cases} V_0(1 - r/\sigma)^2, & r < \sigma, \\ 0, & r \geqslant \sigma, \end{cases} \tag{1}$$

where r is the center-to-center distance between two particles. Length and time are measured in units of σ and $(m\sigma^2/V_0)^{1/2}$, respectively, and V_0 sets the energy scale. We initially place N particles at random in a cubic box of linear dimension L. This corresponds to a $T=\infty$ configuration. We use conjugate-gradient energy minimization [16] in order to obtain $T=0$ configurations.

The onset of jamming in the limit of large N occurs at a packing fraction $\phi_c^{N\to\infty} = 0.639 \pm 0.003$ [7], and is characterized by the onset of a nonzero pressure. We determine ϕ_c for each of our finite-system initial configurations by incrementally compressing (decompressing) until the pressure just becomes nonzero (just reaches zero). We then compress the system to obtain zero-temperature compressed configurations

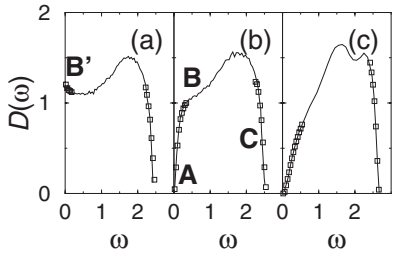

FIG. 1. Density of states $D(\omega)$ of 3D jammed packings of monodisperse spheres at three different compressions $\Delta\phi$=(a) 10^{-6}, (b) 10^{-2}, and (c) 10^{-1}. In (a) we identify regime B', and in (b) we identify the regimes A, B, and C discussed in the text. The lines show data for the systems with $N=1024$. The symbols show the low- and high-frequency portions of $D(\omega)$ for $N=10\,000$. There is no discernible size dependence.

at controlled values of $\Delta\phi \equiv \phi - \phi_c$. For each of these configurations, we compute and diagonalize the dynamical matrix [17]. The eigenvalues and eigenmodes of this matrix are respectively the squared frequencies ω^2 of the normal modes of vibration and the corresponding polarizations $\mathbf{e}_{i_\omega}$ of each particle i in the normal mode of frequency ω.

We studied two system sizes in 3D. For $N=1024$ we generated ten independent initial configurations, hence averaging over ten realizations at each value of $\Delta\phi$. For this system size, $L \approx 10$, we are able to obtain the full vibrational spectrum but remain restricted in the extent of spatial information. To overcome this, we also generated five independent realizations with $N=10\,000$, resulting in $L \approx 20$, from which we are able to extract spatial correlation functions characterizing the modes. For these larger systems we are able to extract only a limited range of the low- and high-frequency portions of the vibrational spectrum. In these frequency ranges, we do not see any system-size dependence in the density of states as indicated in Fig. 1. Additionally, to *visualize* the normal modes, we have also studied $N=10\,000$ bidisperse 50:50 mixtures of harmonic disks with a diameter ratio of 1.4 in 2D.

III. RESULTS

A. Normal mode statistics

In a previous paper [9], we analyzed the density of vibrational states $D(\omega)$ of configurations above the jamming threshold, for systems at $\phi > \phi_c$, and found three characteristic regimes, as labeled in Fig. 1(b). In regime A, $D(\omega)$ decreases toward zero as $\omega \to 0$. In regime B [including B' in Fig. 1(a)], $D(\omega)$ is approximately constant, which is very different than for crystals. Finally, in regime C at high frequencies, $D(\omega)$ decreases with increasing frequency. Figures 1(a)–1(c) shows how the different regimes shift with increasing compression. At high $\Delta\phi$, corresponding to high compressions, regime A extends to fairly high frequencies and regime B is small. As the system is decompressed toward the marginally jammed solid at $\Delta\phi=0$, regime A shrinks and regime B grows, extending all the way down to zero frequency, as indicated by B' in Fig. 1(a), while regime C remains approximately the same. The growth of regime B at the expense of regime A with decreasing compression signals the proliferation of anomalous low-frequency modes. These are the modes whose structure we wish to understand. We also point out that $D(\omega)$ for 2D jammed packings of bidisperse disks exhibits similar behavior to our 3D results [13].

B. Visualization of modes in two dimensions

Because three-dimensional structures are hard to visualize, we turn to a bidisperse two-dimensional system in order to visualize the structure of the modes in each of these regions. Many features of 2D marginally jammed solids are similar to those in 3D [8]. Figure 2 shows typical normal modes from regimes A, B', B, and C, defined in Figs. 1(a) and 1(b), for the equivalent 2D system. In the left panels, the polarization vector for each particle is shown, while in the right panel, each particle is shaded according to the magnitude of its polarization vector. The mode from regime A, Fig. 2 (top), appears to have some plane-wave-like character, although contributions from several different wave vectors are readily apparent. The high-frequency mode corresponding to

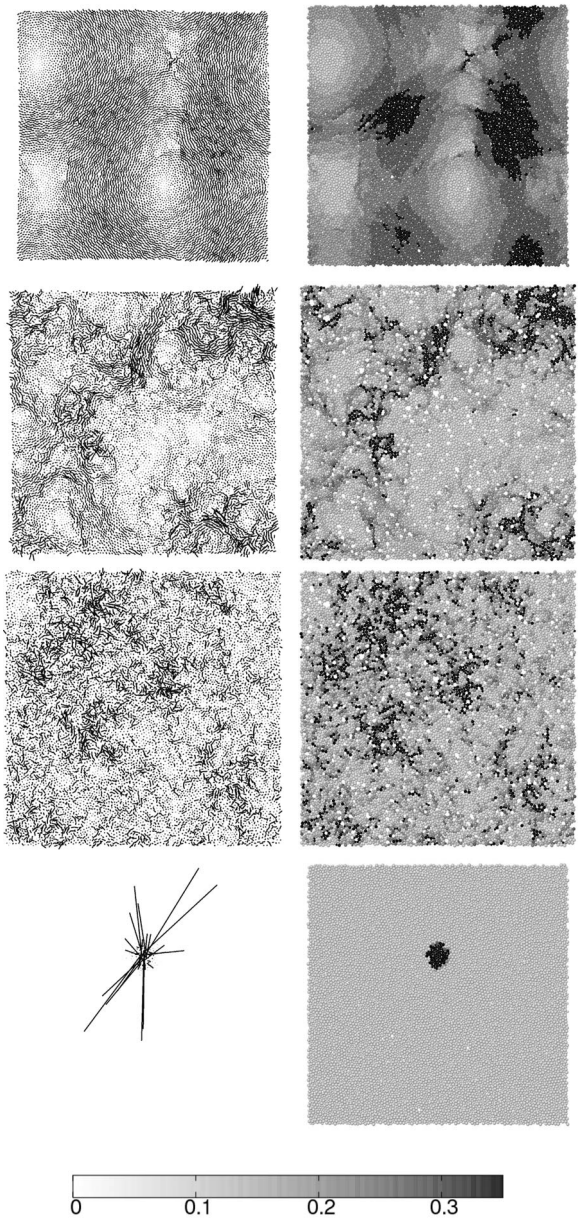

FIG. 2. Visualization of normal modes for a 2D jammed packing where visualization is easier than in 3D. The systems are for a 50:50 mix of $N=10\,000$ bidisperse disks, with size ratio 1:1.4, interacting with the potential defined in Eq. (1). These figures correspond to the regimes identified in Figs. 1(a) and 1(b), characterized by $(\Delta\phi, \omega)$. Top row panels: regime A $(1\times10^{-1}, 1.76\times10^{-2})$. Second row: regime B' $(1\times10^{-6}, 3.35\times10^{-4})$. Third row: regime B $(1\times10^{-6}, 0.3)$. Bottom row: regime C $(1\times10^{-1}, 2.30)$. Left panels: black lines represent the amplitude and direction of the particle vibrations in that mode. Right panels: particles are shaded according to the magnitude of their polarization vector. The scale bar indicates that darker shading corresponds to a larger ratio of the amplitude to the maximum amplitude of particle displacement in that mode. Particles with no contact neighbors are not shown.

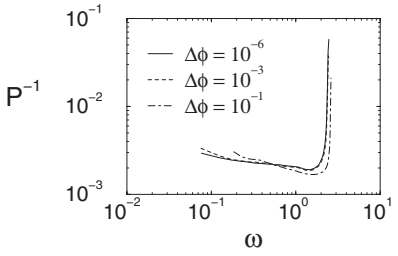

FIG. 3. Inverse participation ratio P^{-1} for 3D jammed packings of $N=1024$ monodisperse spheres, at three compressions. The data are averaged over narrow bins of frequency.

regime C, Fig. 2 (bottom), is highly localized. This particular mode is representative of the high-frequency modes at all values of $\Delta\phi$; visualizations of individual modes at different $\Delta\phi$ in this high-frequency region show similar features to that shown in Fig. 2 (bottom).

The modes from regimes B' and B, Fig. 2 (middle), are neither plane-wave-like nor localized. The right panels more clearly reveal the filamentary nature of the extended vibrational modes in regimes B' and B. These visualizations already suggest some subtle differences between regimes B' and B which we quantify below (see Fig. 7 and related discussion). Figure 2 suggests that the modes from both regimes A and B are extended.

C. Participation ratio

To analyze directly how extended each mode is, we calculate the inverse participation ratio

$$P^{-1} = \frac{\sum_{i=1}^{N} |\mathbf{e}_{i_\omega} \cdot \mathbf{e}_{i_\omega}|^2}{\left| \sum_{i=1}^{N} \mathbf{e}_{i_\omega} \cdot \mathbf{e}_{i_\omega} \right|^2}. \tag{2}$$

Here $\mathbf{e}_{i_\omega}$ is the polarization vector of particle i in the mode ω. We show the results for $\Delta\phi=10^{-6}$, 10^{-3}, and 10^{-1} in Fig. 3. The data shown are averaged over narrow bins of frequency. We find that on a log-log scale the averaged participation ratio looks quite similar for values of $\Delta\phi$ up to at least $\Delta\phi \approx 10^{-3}$. For high compressions ($\Delta\phi=0.1$ and higher), P^{-1} at the very highest frequencies (regime C) appears to decrease with increasing compression, but the average P^{-1} is still large in regime C at all compressions. Thus, the modes in regime C are localized at all compressions. At lower frequencies, however, up to $\omega \approx 2$, we find $P^{-1} \ll 1$, indicating that the modes are extended over the size of the system. Thus, modes in regimes A and B are, on average, extended, while those in regime C are localized.

D. Level repulsion

For these jammed, mechanically stable packings, there exist local correlations in the force constants that constitute the dynamical matrix: The forces around each and every particle must be locally balanced. Upon analyzing the spacings $\Delta\omega=\omega_{j+1}-\omega_j$ between successive normal mode frequencies, we find level repulsion in the distribution of level spacings, $P(s)$, where we define $s=\Delta\omega/\langle\Delta\omega\rangle$ as the level spacing normalized by the average $\langle\Delta\omega\rangle$. The total distributions shown in Fig. 4(a) show little dependence on distance to the jamming threshold, and are described quite well by the Wigner-Dyson distribution [18]

$$P(s) = \frac{\pi s}{2} e^{-\pi s^2/4}. \tag{3}$$

The distributions are peaked around the average spacing and indicate level repulsion by the linear behavior at small spacing consistent with studies in two dimensions [19]. Thus, even though the dynamical matrix is sparse, due to the short-range nature of the interaction potential, the level spacings are not completely random, which would lead to a Poisson distribution, nor are they completely correlated. Note that in Fig. 4(a) all modes have been included, even the localized modes at high frequency. If the localized modes are considered separately, it has been shown in 2D systems that the level spacings are uncorrelated and have a Poissonian distribution [19]. We find consistent results in 3D as shown in Fig. 4(b).

E. Correlations in normal modes

Another way to characterize the modes is to look at local correlations of the polarizations of neighboring particles. We calculate a quantity, $\cos\theta_e$, that is similar to the phase quotient parameter often probed in glasses [20],

$$\cos\theta_e(\omega) = \frac{1}{N_{\text{pairs}}} \sum_{i,j} \hat{\mathbf{e}}_{i_\omega} \cdot \hat{\mathbf{e}}_{j_\omega} \tag{4}$$

where the sum only runs over the number of pairs of particles that interact with each other, N_{pairs}, and the normalized polarization vector of particle i associated with the normal mode of frequency ω, $\hat{\mathbf{e}}_{i_\omega}=\mathbf{e}_{i_\omega}/|\mathbf{e}_{i_\omega}|$. For a mode in which

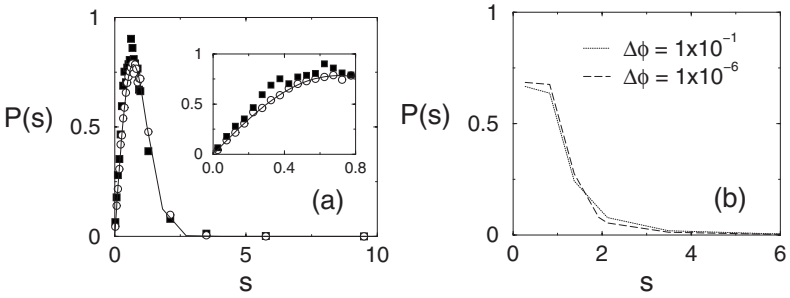

FIG. 4. Distribution $P(s)$ of level spacings s normalized by the average level spacing for $N=1024$ monodisperse spheres in 3D. (a) The distribution for all modes in the system at $\Delta\phi=10^{-1}$ (■) and 10^{-6} (○). Inset: linear behavior at small s. The lines are fits to the Wigner-Dyson function of Eq. (3). (b) The distribution for only the localized modes at high frequency.

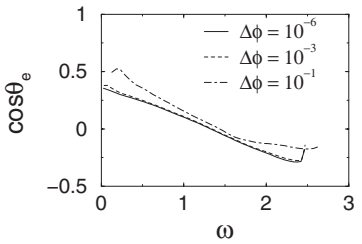

FIG. 5. Correlation between particle displacements in a mode, measured using cos θ_e defined by Eq. (4), at three compressions for 3D jammed packings with $N=1024$ monodisperse spheres.

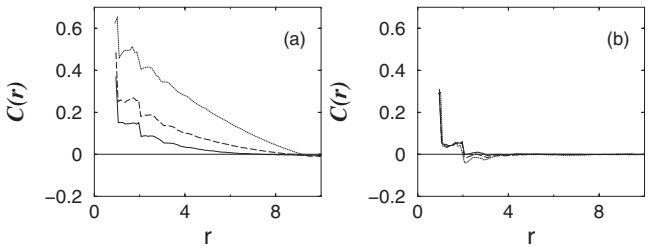

FIG. 6. Spatial correlation function $\mathcal{C}(r)$ of particle vibrations at three values of $\Delta\phi=10^{-6}$ (solid line), 10^{-2} (dashed), and 10^{-1} (dotted), for $N=10\,000$ monodisperse spheres in 3D, averaged over (a) the ten lowest-lying frequency modes, and (b) ten modes at intermediate frequencies $\omega\sim 0.5$.

every particle is vibrating in approximately the same direction, i.e., strongly correlated motion, one would expect $\cos\theta_e \approx 1$. Figure 5 shows $\cos\theta_e$ as a function of frequency at three values of $\Delta\phi$. Up to compressions of order $\Delta\phi = 10^{-3}$, the behavior of $\cos\theta_e$ with ω is insensitive to compression. Over that range of compressions, $\cos\theta_e$ decreases linearly with increasing frequency, showing that in the low-frequency modes particle displacements are more correlated with their neighbors and in high-frequency modes particle displacements are more anticorrelated with their neighbors. Note that the frequency ranges of regimes A and B change appreciably with $\Delta\phi$, while $\cos\theta_e(\omega)$ does not; this suggests that the correlations are not noticeably different in the two regimes. At high compressions, the curve begins to show a kink at approximately $\omega=1.75$ (the boundary between regimes B and C).

By visual inspection of the 2D modes of Fig. 2, the low-frequency modes both near and far from the jamming threshold appear to have somewhat different character. We contend that compressed systems away from the jamming threshold contain low-frequency modes that are more plane-wave-like, whereas near the jamming transition, these extended modes are very different from plane waves. At intermediate and high frequencies the modes appear relatively insensitive to packing fraction. In an effort to further differentiate between the natures of the low-frequency modes we measure the spatial extent of correlated vibrational motions. For each mode of frequency ω, we compute the correlation of polarization vectors between particles i and j,

$$\mathcal{C}(r_{ij}) = \langle \hat{\mathbf{e}}(\mathbf{r}_i) \cdot \hat{\mathbf{e}}(\mathbf{r}_j) \rangle. \tag{5}$$

In Fig. 6 we show $\mathcal{C}(r)$ for the lowest-lying frequency modes and those at intermediate frequencies, at three different compressions $\Delta\phi=10^{-6}$, 10^{-2}, and 10^{-1} for our 3D jammed packings.

For the low-frequency modes, Fig. 6(a), we find somewhat stronger correlations at higher compressions. For the middle to high-frequency range of the vibrational spectrum, beyond regime A, Fig. 6(b), the normal modes become increasingly similar at different compressions. In regime C, the modes are indistinguishable at different compressions.

All of the correlation functions in Fig. 6 decay nonmonotonically to zero and cross zero at some finite r. We define the value of r at which $\mathcal{C}(r)$ first crosses zero to be $\ell(\omega)$. In a pure plane wave, particle vibrations are correlated and $\mathcal{C}(r)$ will cross zero at the scale of half the wavelength, so for ordinary sound modes at low frequency, one would expect $\ell(\omega) \propto 1/\omega$. In Fig. 7, we plot ℓ as a function of ω for different $\Delta\phi$ at low to intermediate frequencies. For the system closest to the jamming threshold, ℓ is approximately independent of ω at very low frequencies. Beyond this constant region, ℓ decreases with increasing frequency, corresponding to moving along the plateau in the density of states from regime B' to B [21]. As the system moves further from the jamming threshold, i.e., as $\Delta\phi$ increases, the region of constant ℓ shrinks. Over the range of frequencies where ℓ decreases, the characteristic length is greater the further the system is from the jamming threshold. This is to be expected as the modes contain more plane-wave character at larger compressions. At slightly higher frequencies still, the curves begin to overlap, indicating that the modes become practically indistinguishable. The frequency at which this occurs coincides with the point in the density of states where the plateau regions start to merge (see Fig. 1 of Ref. [9]). These data suggest that the distinction between modes from regimes B' and B is related to how extended the modes are. This is already evident from the visualizations presented in Fig. 2.

F. Dispersion behavior

Another way to quantify the difference between the extended modes in regimes A and B is through the Fourier transforms of the eigenmodes at different frequencies ω throughout the spectrum. Specifically, we take the Fourier transform of the appropriate component, either longitudinal

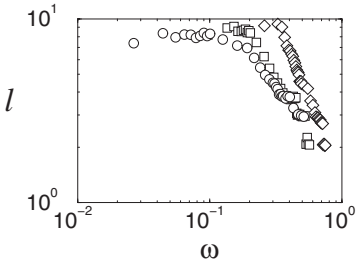

FIG. 7. Dependence of the characteristic length scale ℓ, defined in text, on the normal mode frequency ω, at three values of $\Delta\phi = 10^{-6}$ (○), 10^{-3} (□), and 10^{-1} (◇), for $N=10\,000$ monodisperse spheres in 3D.

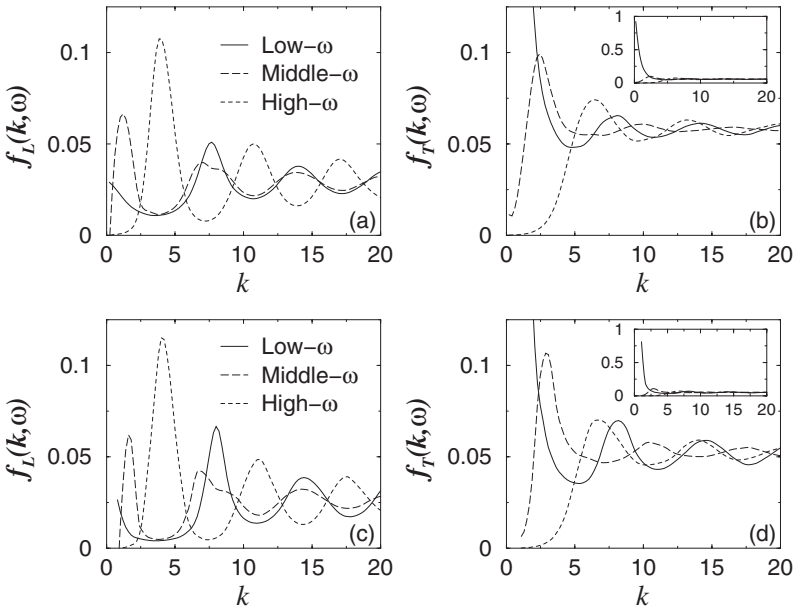

FIG. 8. Fourier transforms of the eigenmodes for the low- (solid line), middle- (dashed line), and high- (dotted line) frequency regions of the vibrational spectrum, at two extreme compressions for $N=1024$ monodisperse spheres in 3D. Top panels: $\Delta\phi=1\times10^{-6}$, for the (a) longitudinal and (b) transverse components. Bottom panels: $\Delta\phi=1\times10^{-1}$, for the (c) longitudinal and (d) transverse components. Insets to (b) and (d) show the dominance of the low-k peak in the transverse functions.

or transverse, of the particle polarization vector $\mathbf{e}_j(\omega)$ of each particle j [3,9]:

$$f_L(k,\omega) = \left\langle \frac{1}{N}\left|\sum_j \hat{\mathbf{k}}\cdot\mathbf{e}_{j_\omega}\exp(\imath\mathbf{k}\cdot\mathbf{r}_j)\right|^2\right\rangle,$$

$$f_T(k,\omega) = \left\langle \frac{1}{N}\left|\sum_j \hat{\mathbf{k}}\wedge\mathbf{e}_{j_\omega}\exp(\imath\mathbf{k}\cdot\mathbf{r}_j)\right|^2\right\rangle. \quad (6)$$

In a perfect crystal, these functions would be δ functions at the wave numbers k in each Brillouin zone characterizing the longitudinal or transverse vibrational modes at frequency ω. In Fig. 8, we show $f_L(k,\omega)$ and $f_T(k,\omega)$ curves for two disordered configurations in three frequency bands: (i) at the lowest frequency, (ii) in the middle of the band, and (iii) at the high-frequency end of the spectrum. Each curve is averaged over a narrow bin of frequencies. For comparison, Figs. 8(a) and 8(b) are from a system very close to the jamming threshold, at $\Delta\phi=10^{-6}$, and Figs. 8(c) and 8(d) are for a system that is highly compressed and far from the jamming threshold, at $\Delta\phi=10^{-1}$. At $\Delta\phi=10^{-6}$, the low- and mid-frequency curves correspond to vibrational states in regime B' defined in Fig. 1(a), where the density of states is relatively flat, while the high-frequency curve corresponds to regime C. At high compression, $\Delta\phi=10^{-1}$, the low-frequency curve corresponds to a state in regime A, the mid-frequency curve corresponds to regime B, and the high-frequency curve corresponds to regime C.

The longitudinal functions in general show much more pronounced structure than do their transverse counterparts. The only exception to this occurs at very low frequencies and small wave vectors. In this region the transverse function has a very tall first peak and the longitudinal function shows only a hint of structure. The low-wave-vector part of the peak in $f_T(k,\omega_{\text{low}})$ is not resolved because it occurs at $k<2\pi/L$ where L is the size of the system. That is, the peak is cut off because of the finite size of the system. The first peak in $f_L(k,\omega_{\text{low}})$ is also absent for the same reason. In order to see this structure, one would have to either use a larger box size at the same value of frequency or else look at $f_L(k,\omega)$ at a larger value of ω.

There are multiple oscillations visible in the longitudinal response $f_L(k,\omega)$. This structure can be thought of as the equivalent of the repeated structure seen in the higher Brillouin zones of a crystal [3]. It reflects the large, sharp first peak in the pair-correlation function $g(r)$ [22], which leads to strong oscillations in the structure factor $S(k)=\langle|\Sigma_i\exp(\imath\mathbf{k}\cdot\mathbf{r}_i)|^2\rangle$ [8]. Similar oscillations show up but with a very much smaller amplitude in $f_T(k,\omega)$.

Overall, the results look fairly similar for the two compressions, although individual packings exhibit fluctuations about the averaged behavior. For the longitudinal response, the peaks are somewhat smaller and wider at low compression. However, the most obvious difference is not in the peaks but in the minima between them, which become shallower at small $\Delta\phi$. This is particularly apparent at the lower frequencies in the longitudinal response. This means that more wave vectors are making significant contributions to the low-frequency longitudinal modes at low compression (which are in regime B) than to low-frequency longitudinal modes at high compression (which are in regime A), making the mode very different from any plane wave with a single wave vector. A similar trend is apparent in the transverse response. Contributions of wave vectors different from the peak value are relatively larger at low compressions; that is, more wave vectors contribute to eigenmodes in regime B than in regime A. The intermediate wave-vector oscillations, clearly visible at $\Delta\phi=10^{-1}$, are much less pronounced near the onset of jamming. At low frequency, the transverse response is practically flat at wave vectors $k>5$—all of these high wave vectors contribute nearly equally in regime B [23].

The velocity of longitudinal or transverse sound can be estimated from the frequency dependence of the position of the first peak in $f_L(k,\omega)$ or $f_T(k,\omega)$. Unlike in crystals, the dispersion curve is not well defined at the frequencies represented here because, as we have seen in Fig. 8, $f_L(k,\omega)$ and

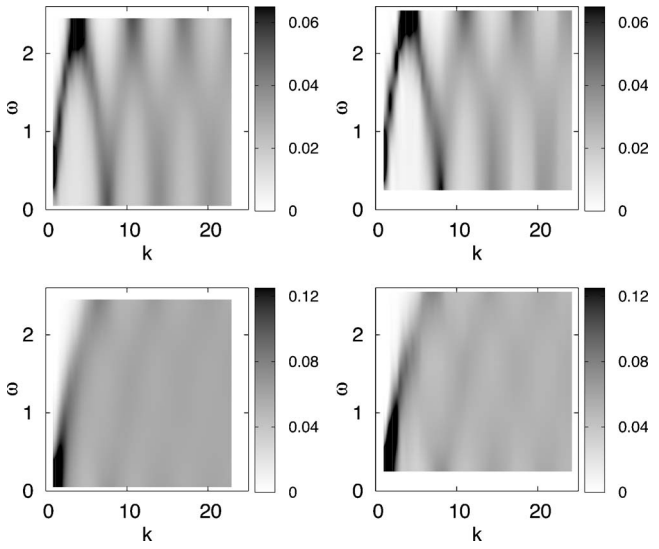

FIG. 9. Dispersion relation at two different compressions for $N=1024$ monodisperse spheres in 3D. Left panels: $\Delta\phi=1\times10^{-6}$. Right panels: $\Delta\phi=1\times10^{-1}$. Top and bottom panels correspond to longitudinal and transverse modes, respectively. Darker shading corresponds to larger amplitude in $f_{L,T}$. The maxima of the transverse amplitudes are typically a factor of 5 larger than for the longitudinal data. The bars to the right indicate the amplitude scale.

$f_T(k,\omega)$ have significant amplitude over a large range of wave vector at all frequencies. As a result, it is not sufficient to simply plot the positions of the peaks of the dynamic structure factors as one might do for a crystal. Only at very low values of ω, below what is shown for these finite-size samples, do the dispersion curves have sharp peaks corresponding to sound waves.

To emphasize the idea of mode mixing, the dispersion data are best visualized on a gray scale plot as shown in Fig. 9. (The features outlined here have been seen in a range of glassy systems, including soft-sphere [24], covalent [25], and metallic [26] glasses.)

Because the amplitude of the first peak in $f_T(k,\omega)$ is so strong, variations at wave vectors greater than the first peak are lost in Fig. 9. Therefore, to observe the underlying structure in the dispersion data at larger wave vectors, in Fig. 10 we show the transverse dispersion curves over a limited range in amplitude. These nicely contrast the unusual underlying structure to the dispersion relations at the two compressions.

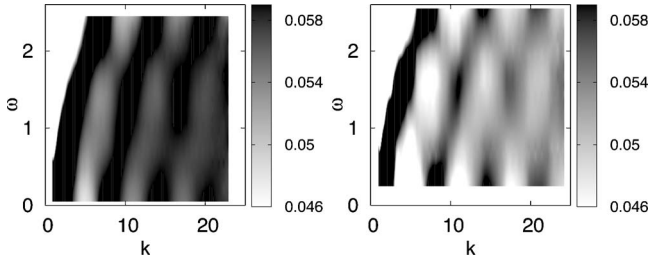

FIG. 10. Transverse dispersion data of Fig. 9 for $\Delta\phi=1\times10^{-6}$ (left) and 1×10^{-1} (right), over a limited range in amplitude f_T (see scale bar).

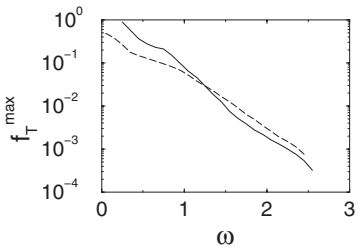

FIG. 11. Decay of the peak maximum of the transverse mode transforms within the first Brillouin zone, for $\Delta\phi=10^{-1}$ (solid line) and 10^{-6} (dashed line). For $N=1024$ in 3D.

It is clear from looking at these plots that the dispersion relations are very broad indeed, especially at low compression. Moreover, there is very little difference between the two compressions, although the contrast decreases for both transverse and longitudinal modes with decreasing compression. The limit of what we can achieve is $\Delta\phi=10^{-6}$. It is not clear to us whether the variations in $f_T(k,\omega)$ would disappear entirely if one were able to go even closer to $\Delta\phi=0$.

It is also unclear how to define a proper velocity of sound, not only because the peaks in the dispersion relations are so broad, but also because their amplitudes decay rapidly with increasing (k,ω). We illustrate this latter point in Fig. 11 where we show the approximately exponential decay of the maximum peak height of the transverse Fourier modes with increasing frequency. We have been unable to determine precisely whether the decay constant depends on compression; although there appears to be a difference between the two compressions shown in Fig. 11, that difference is small.

IV. CONCLUSIONS

In summary, we have studied the characteristics of vibrational modes as a function of frequency at different compressions. From the density of states, we see that there are three regimes: regime A, where the density of states drops towards zero as the frequency goes to zero; regime B, where the density of states is approximately flat; and regime C, where the density of states decreases toward zero with increasing frequency. As the system is decompressed toward the marginally jammed state, regime B (or B') increases at the expense of regime A while regime C is relatively unaffected. Modes from regime C are localized while modes from regimes A and B are extended. Those in regime A are somewhat more like plane waves, with slightly narrower peaks in the dynamic structure factor, compared to those in regime B. Generally, however, we do not observe strong differences between modes from regimes B and A. Thus, we conclude that the change in the nature of the modes with decreasing compression is much less dramatic than the change in the density of vibrational states.

This result is surprising in the context of the theory of the vibrational properties by Wyart *et al.* [10]. In that theory, the change in the density of states as one raises the frequency from regime A to regime B heralds the onset of a new type of vibrational mode, an "anomalous mode," which is very different in character from the plane-wave-like modes expected

in regime *A*. In contrast, we observe that the modes are not strongly plane-wave-like even in regime *A*. Xu *et al.* [5] find that for the model studied in this paper the onset of the plateau in the spectrum (crossover from regime *A* to *B*) does not correspond to any noticeable change in the transport properties, consistent with our results. However, Xu *et al.* [5] find that in a related "unstressed model," in which the potential is replaced by harmonic springs at their equilibrium length, the change in the vibrational spectrum coincides with a change in the transport properties of the modes, as expected theoretically [10]. In stressed systems, such as those studied here, it is possible that the modes might change character and resemble plane waves more strongly at lower frequencies in some regime A' below regime *A*, inaccessible in our finite-size systems. Work on energy transport in the same model [5] suggests that this may occur.

ACKNOWLEDGMENTS

We thank T. Witten for helpful discussions. We gratefully acknowledge the support of Grant No. NSF-DMR-0087349 (A.J.L.), NSF MRSEC Grant No. DMR-0213745 (S.R.N.), and DOE Grant Nos. FG02-03ER46087 (A.J.L., L.E.S.) and FG02-03ER46088 (S.R.N., L.E.S.).

[1] R. J. Bell, in *Methods in Computational Physics: Advances in Research and Applications*, edited by G. Gilat (Academic, New York, 1976), Vol. 15, p. 216.
[2] S. John, H. Sompolinsky, and M. J. Stephen, Phys. Rev. B **27**, 5592 (1983).
[3] G. S. Grest, S. R. Nagel, and A. Rahman, Phys. Rev. Lett. **49**, 1271 (1982).
[4] *Amorphous Solids, Low Temperature Properties*, edited by W. A. Phillips (Springer, Berlin, 1981).
[5] N. Xu, V. Vitelli, M. Wyart, A. J. Liu, and S. R. Nagel, Phys. Rev. Lett. **102**, 038001 (2009).
[6] D. J. Durian, Phys. Rev. E **55**, 1739 (1997).
[7] C. S. O'Hern, S. A. Langer, A. J. Liu, and S. R. Nagel, Phys. Rev. Lett. **88**, 075507 (2002).
[8] C. S. O'Hern, L. E. Silbert, A. J. Liu, and S. R. Nagel, Phys. Rev. E **68**, 011306 (2003).
[9] L. E. Silbert, A. J. Liu, and S. R. Nagel, Phys. Rev. Lett. **95**, 098301 (2005).
[10] M. Wyart, S. R. Nagel, and T. A. Witten, Europhys. Lett. **72**, 486 (2005).
[11] M. Wyart, L. E. Silbert, S. R. Nagel, and T. A. Witten, Phys. Rev. E **72**, 051306 (2005).
[12] A. R. Abate and D. J. Durian, Phys. Rev. E **74**, 031308 (2006).
[13] W. G. Ellenbroek, E. Somfai, M. van Hecke, and W. van Saarloos, Phys. Rev. Lett. **97**, 258001 (2006).
[14] T. S. Majmudar, M. Sperl, S. Luding, and R. P. Behringer, Phys. Rev. Lett. **98**, 058001 (2007).
[15] L. E. Silbert, C. S. O'Hern, A. J. Liu, and S. R. Nagel, in *Unifying Concepts in Granular Media and Glasses*, edited by A. Coniglio, A. Fierro, H. J. Herrmann, and M. Nicodemi (Elsevier, Amsterdam, 2004), p. 1.
[16] W. H. Press, B. P. Flannery, S. A. Teukolsky, and W. T. Vetterling, *Numerical Recipes in Fortran 77* (Cambridge University Press, New York, 1986).
[17] N. W. Ashcroft and N. D. Mermin, *Solid State Physics* (Brooks/Cole, London, 1976).
[18] M. L. Mehta, *Random Matrices and the Statistical Theory of Energy Levels* (Academic, New York, 1967).
[19] Z. Zeravcic, W. van Saarloos, and D. R. Nelson, Europhys. Lett. **83**, 44001 (2008).
[20] P. B. Allen, J. L. Feldman, J. Fabian, and F. Wooten, Philos. Mag. B **79**, 1715 (1999).
[21] Over the limited range of data, the initial decay approximately follows $\ell \sim 1/\omega$.
[22] L. E. Silbert, A. J. Liu, and S. R. Nagel, Phys. Rev. E **73**, 041304 (2006).
[23] It would be interesting to study how the these modes differ from acoustic plane waves using larger systems to probe lower wave numbers.
[24] H. R. Schober, J. Phys.: Condens. Matter **16**, S2659 (2004).
[25] O. Pilla, L. Angelani, A. Fontana, J. R. Goncalves, and G. Ruocco, J. Phys.: Condens. Matter **15**, S995 (2003).
[26] J. Hafner, Phys. Rev. B **27**, 678 (1983).